MDPI

Article

Mechanism and Design Method of Load Transfer into Concrete-Filled Steel Tubular Arch Ribs through Perfobond-Rib-Shear Connectors

Yongjian Liu [1,2], Jiangjiang Li [1], Lei Jiang [1,*], Jianping Xian [3], Haotian Li [3], Yadong Zhao [1] and Yunxia Gong [1]

[1] School of Highway, Chang'an University, Xi'an 710064, China; liuyongjian@chd.edu.cn (Y.L.); lijiangjilin@chd.edu.cn (J.L.); 2022021026@chd.edu.cn (Y.Z.); 2021121069@chd.edu.cn (Y.G.)
[2] School of Civil Engineering, Chongqing University, Chongqing 400044, China
[3] Engineering Design and Research Institute of CCCG Second Highway Engineering, Xi'an 710199, China; 20190622@ccccltd.cn (J.X.); lihaotian@ccccltd.cn (H.L.)
*   Correspondence: jiangleichd@chd.edu.cn

Abstract: In terms of load transfer, the design of the joints in concrete-filled steel tubular (CFST) arch bridges is more critical than that in buildings due to the higher likelihood of steel–concrete-interface debonding. To improve the contact at the steel–concrete interface, a novel arch rib was manufactured by longitudinally welding perfobond-rib-shear connectors to the inner surface of a steel tube and then filling the tube with concrete. In this study, extensive numerical and analytical investigations on the mechanism of introducing loads into CFST arch ribs through perfobond-rib-shear connectors were carried out. A deck CFST arch bridge, namely, the Shuangbao Bridge in China, was selected as a typical application location. The design parameters, including the geometric dimensions of the perfobond-rib-shear connector and the arrangement of the perfobond rib along the cross-section and longitudinal section of the arch rib, were evaluated. The design flow for the joint with perfobond-rib-shear connectors between the vertical columns and the CFST arch ribs was proposed. To improve the load-transfer efficiency, the design scheme of the joint in the Shuangbao Bridge was optimized by replacing the weld studs with perfobond ribs. Significant increases of 1.84–4.02 in the shear resistance were found for the perfobond ribs compared to the welded studs. Additionally, the fabrication of the perfobond ribs was more convenient compared to that of the welded studs.

Keywords: concrete-filled steel tubular arch bridge; perfobond-rib-shear connector; load transfer; design method; bond strength; steel–concrete interface

1. Introduction

In the past 20 years, due to their excellent structural performance and attractive appearance, more than 400 concrete-filled steel tubular (CFST) arch bridges have been constructed in China [1,2], and specific design guidelines for CFST arch bridges have been issued. However, there are still some difficulties in the design of CFST arch bridges. In the practical engineering process, the vertical column and hanger anchor system are directly connected to the outer surface of the CFST arch rib. In this case, the load is applied to the steel tube first and then transferred to the concrete core by a steel–concrete bond through an "introduction length" to fulfill the composite action. Additionally, in consideration of the confinement effect, the hoop stress of the steel tube increases while the allowable longitudinal stress decreases, in compliance with the von Mises yield criterion, leading to the premature failure of the steel tube [3–6]. Therefore, it is critical to create a reasonable design of the joint between the vertical column (or hanger anchor system) and CFST arch rib to guarantee the load transfer.

Wang et al. [7], Dong et al. [8], and Naghipour et al. [9] investigated the bond strengths of CFST columns using push-out tests. It was demonstrated that the bond strength between

the steel tube and the concrete core must be very small to result in a longer load-transfer time. Furthermore, for interface debonding, the load cannot be effectively introduced into the concrete core. For the design of beam–column joints in buildings, it is much easier to guarantee the load transfer. Shear connectors, such as gusset plates, bearing rings, and stiffeners, are normally placed within the inner surface to transfer the beam reaction, while the quality of the concrete in CFST structures in buildings is less affected by the ambient temperature, meaning a reliable steel–concrete bond can be easily obtained [10–18]. However, for the design of joints between vertical columns and CFST arch ribs, it is difficult to guarantee the load transfer. On one hand, the shear force applied to the arch rib is larger than that in the building. On the other hand, it was proven that steel–concrete-interface debonding is more likely in CFST arch bridges than in CFST buildings because of the concrete shrinkage and creep that occur due to the complications of ambient temperatures [19,20].

To address this problem, a novel arch rib was manufactured by Liu et al. by longitudinally welding perfobond ribs to the inner surface of a steel tube and then filling the tube with concrete, namely a CFST arch rib stiffened with perfobond ribs [21,22]. Additionally, Jiang et al. [23–27] and Cheng et al. [28] conducted extensive studies on these novel structures in terms of the steel–concrete-interface behavior, the buckling behavior of the steel tube, the confinement effect of the member, and the static and fatigue behavior of the joint. It was found that the perfobond ribs worked as both stiffeners and shear connectors, as follows: (1) as the stiffener, the perfobond rib improved the buckling resistance of the steel tube, reduced the stress concentration of the joint, and enhanced the confinement effect of the arch rib; (2) as the shear connector, the perfobond rib significantly enhanced the steel–concrete bond and prevented the steel–concrete interface from debonding under temperature changes.

Based on the studies mentioned above, in this paper, we further study the mechanism for introducing loads into CFST arch ribs through perfobond-rib-shear connectors. A typical application scenario of Shuangbao Bridge in China was selected as the research object and the design parameters are evaluated, namely the geometric dimensions of the perfobond rib and the arrangement of the perfobond rib along the cross-section and longitudinal section of the arch rib. The design flow for the novel joint with perfobond rib-shear-connectors is provided.

2. Literature Review on the Bond Behaviors of CFST Columns

To date, scholars have conducted numerous studies on the steel–concrete bonding of CFST columns. Meanwhile, some design guidelines have provided bond-behavior models for the beam–column joints in buildings. A thorough understanding of the bond behaviors of CFST columns is helpful to reveal the load-transfer mechanism of CFST arch ribs. Therefore, in the following sections, we will review the experimental research on steel–concrete bonds and the bond-behavior models recommended by the design guidelines.

2.1. Experimental Study on Steel–Concrete Bonds

Figure 1 illustrates the typical bond stress–slip curves at the steel–concrete interface. It has been demonstrated that the bond strength is composed of three parts: chemical adhesion, physical interlocking (also called micro-interlocking), and frictional resistance (also called macro-interlocking) [29]. As shown in Figure 1a, the typical bond stress–slip curve has a significant peak point at the end of stage I. This is because the initial frictional resistance is lower than the sum of the chemical adhesion and physical interlocking, meaning a drop in the bond stress can be observed after the chemical bond is broken. Additionally, three kinds of curve, such as a, b, and c, are present, depending on the magnitude of the frictional resistance. Conversely, Figure 1b illustrates the typical bond stress–slip curve without a peak point at the end of stage I. This indicates that the initial frictional resistance is larger than the sum of the chemical adhesion and physical interlocking, which can normally be found in the push-out test with a smooth steel–concrete interface.
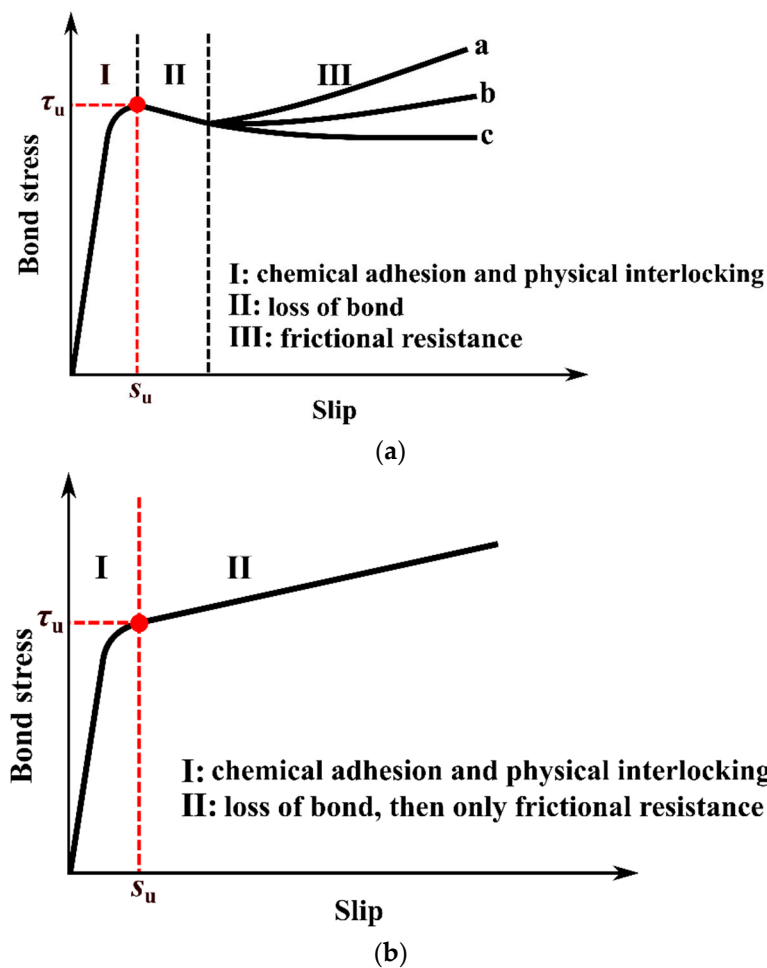
Figure 1. Typical bond stress–slip curves at the steel–concrete interface: (**a**) the curve with peak point; (**b**) the curve without peak point.

In general, the maximum bond stress at the end of stage I (the point of bond loss) is defined as the bond strength τ_u. At stage I, an approximately linear relationship between bond stress and relative slip can be found; therefore, the tangent slope in this stage can be defined as the shear modulus. Table 1 [30–38] lists a summary of the push-out test results of CFST columns. High scatter values were found for the measured bond strength in the range of 0.01–3.65 MPa due to the influence of factors such as the specimen dimensions, smoothness of the steel–concrete interface, concrete strength, concrete age, etc. For the shear modulus, only Liu et al. [37,38] provided the value of 0.165 MPa.

Table 1. Summary of the push-out-test results for CFST columns.

Ref.	Number of Specimens	Dimensions (mm)			Concrete Strength (Mpa)	Bond Strength τ_u (Mpa)	Shear Modulus (Mpa)
		Diameter	Thickness	Height			
Virdi et al. [30]	91	148.4~306	5.6~10.1	149.4~463.6	22.0~46.3	0.27~3.65	/
Roeder et al. [31]	20	247.6~598.4	5.6~13.5	758.0~1927.0	27.9~47.3	0.01~0.79	/
Aly et al. [32]	7	114.3	3.2	450.0	40.0~80.0	0.61~1.23	/
Tao et al. [33]	5	120.0~400.0	3.6~8.0	600.0~1200.0	42.0~55.8	0.60~1.85	/
Xu et al. [34]	3	150.0	2.8~4.5	500.0	47.0	0.60~0.67	/
Xue et al. [35,36]	32	165.0	5.0	300.0~900.0	41.9~83.7	0.37~1.03	/
Liu et al. [37,38]	15	115.0	4.0	345.0~632.0	32.3	0.93~1.41	0.165

2.2. Bond-Behavior Model in Design Guidelines

Table 2 summarizes the bond-behavior models for beam–column joints in buildings recommended by the design guidelines, where *L* is the length of the CFST column, and *D*

is the diameter of the steel tube. In consideration of the effect of the high scatter on the measured bond strength, lower values are usually taken as the design value of the bond strength τ_d in current design guidelines. Among those, the most conservative value of τ_d is 0.23 MPa, as specified in DBJ/T13-51-2010. Furthermore, the steel–concrete contact area for load transfer should be known; it is determined by the bond-transfer length l_x, the bond-transfer circumference, l_{uz}, and the region of the introduction, for which only Eurocode 4 and ANSI-AISC 360-05 provide the relevant provisions.

Table 2. Summary of the bond-behavior models for beam–column joints in buildings, as recommended by design guidelines.

Design Guidelines	Design Value of the Bond Strength τ_d (MPa)	Bond Transfer Length l_x (m)	Region of the Load Introduction	Bond Transfer Circumference l_z (m)
DBJ/T13-51-2010 [39]	0.23	/	/	/
Eurocode 4 [40]	0.55	min (1/3L, 2D)	/	πD
BS5400-5 [41]	0.40	/	/	/
AS5100.6-2004 [42]	0.40	/	/	/
ANSI-AISC 360-05 [43]	0.40	4D	symmetric distances above and below the joint	$\pi D/4$

3. Mechanism of Load Introduction into CFST Arch Ribs through Steel–Concrete Bond

3.1. Force–Equilibrium Relationship in the Load Transfer

The connection between the vertical column and the CFST arch rib in the deck arch bridge is taken as a typical joint. Figure 2 illustrates the force–equilibrium relationship for the load transfer in this typical joint. The curved-arch axis in the region of the introduction length can be assumed as a straight line. Furthermore, the *x*, *y*, and *z* directions are assumed to run along the arch axis, perpendicular to the arch axis, and perpendicular to the plane, respectively.
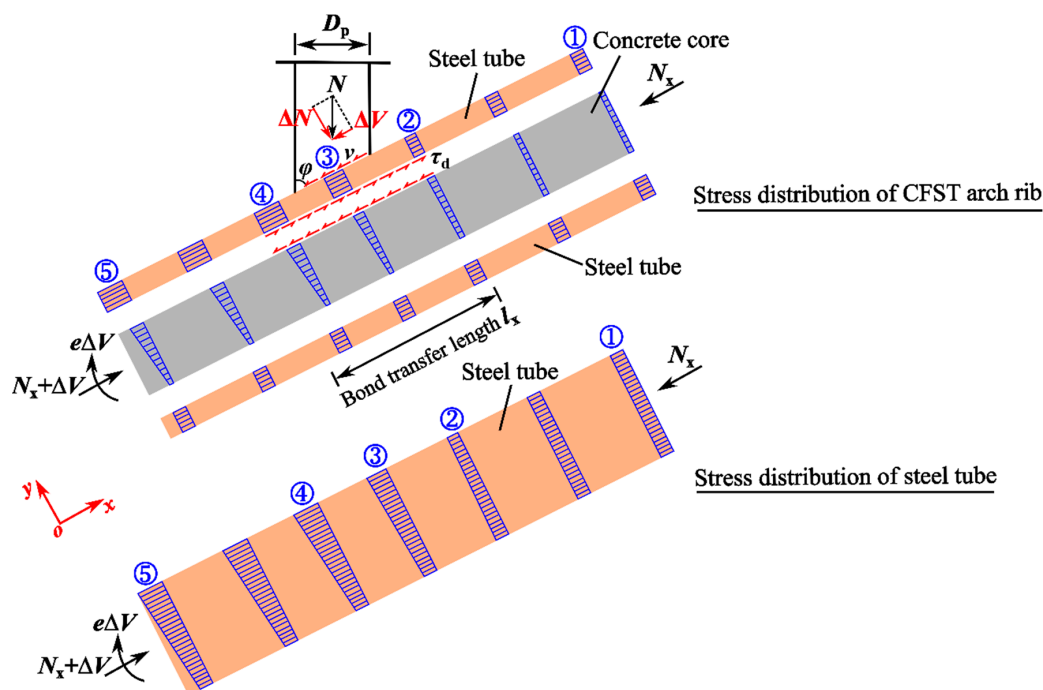

Figure 2. Force–equilibrium relationship for the load transfer at the typical joint of the deck CFST arch bridge.

As shown in Figure 2, the CFST arch rib in the cross-section ① bears the axial force, N_x, which is transferred from the vertical column above this cross-section. Meanwhile, the steel tube and concrete core work together to resist the axial force based on the deformation-compatibility principle. Uniformly distributed compressive stresses can be found on the steel tube (σ_{s1}) and concrete core (σ_{c1}), respectively, in compliance with the axial-stiffness ratio, as follows:

$$\sigma_{s1} = \frac{E_s N_x}{E_s A_s + E_c A_c} \tag{1}$$

$$\sigma_{c1} = \frac{E_c N_x}{E_s A_s + E_c A_c} \tag{2}$$

where E_s and E_c are the elastic moduli of the steel and concrete, respectively, and A_s and A_c are the cross-sectional areas of the steel tube and concrete core, respectively.

The vertical load N transferred from the deck system is directly applied to the outer surface of the steel tube, which can be divided into vertical and horizontal force components (ΔN and ΔV), as presented in Figure 2. It is assumed that the horizontal force component ΔV is uniformly distributed on the top face of the steel tube within the length of the intersection line between the vertical column and the CFST arch rib. Thus, the shear stress v can be determined as follows:

$$v = \frac{\Delta V}{A_p} \tag{3}$$

where $A_p = D_p l_w / \sin\varphi$ is the top face area of the steel tube along the length of the intersection line between the vertical column and the CFST arch rib, which is an arc-sectional area; D_p is the height of the cross-section of the vertical column, as shown in Figure 2; l_w is the arc width of the cross-section of the vertical column; φ is the angle between the vertical column and the CFST arch rib.

The shear stress v applied to the steel tube is transferred to the concrete core through the steel–concrete interface with an arc area A_T, leading to different strains on the steel tube and concrete core in the x-direction. The shear stress at the steel–concrete interface can be taken as the design value of the bond strength τ_d, and the area of the contact surface A_T can be expressed as follows:

$$A_T = l_x l_z \tag{4}$$

At the location below the load-transfer region, the steel tube and concrete core can work together again with the same strain. At this point, the horizontal force applied to the concrete ΔV_c can be calculated as follows:

$$\Delta V_c = \frac{E_c A_c}{E_s A_s + E_c A_c} \Delta V \tag{5}$$

The ΔV_c is equal to the sum of the shear stresses on the contact surface, as follows:

$$\Delta V_c = A_T \tau_d \tag{6}$$

According to Eurocode 4 and ANSI-AISC 360-05 (see Table 2), only the steel–concrete interface on the top face of the steel tube can transfer the shear stress, and the bond-transfer length l_x is greater than the intersection-line length of $D_p / \sin\varphi$. Therefore, the same compressive stress σ_{s1} can be found for cross-sections ①–⑤ on the bottom face of the steel tube. It is assumed that the positive axial force places the member in a tensile state and vice versa. The compressive stress for cross-section ② on the top face of the steel tube (σ_{s2}) decreases because the shear stress is transferred through a distance of Δl_x:

$$\sigma_{s2} = \sigma_{s1} - \frac{\tau_d \Delta l_x}{T} \tag{7}$$

where T is the thickness of the steel tube.

For the cross-section ② of the concrete core, the shear stress τ_d is only transferred to the top face, which is equivalent to an eccentric force applied to the concrete core. The compressive stresses on the top and bottom faces (σ_{c2t} and σ_{c2b}) can be determined by taking a segment Δl_x (see Figure 3) of the concrete core as follows:

$$\sigma_{c2t} = \sigma_{c1} + \frac{4\tau_d \Delta l_x}{H_c} \tag{8}$$

$$\sigma_{c2b} = \sigma_{c1} - \frac{2\tau_d \Delta l_x}{H_c} \tag{9}$$

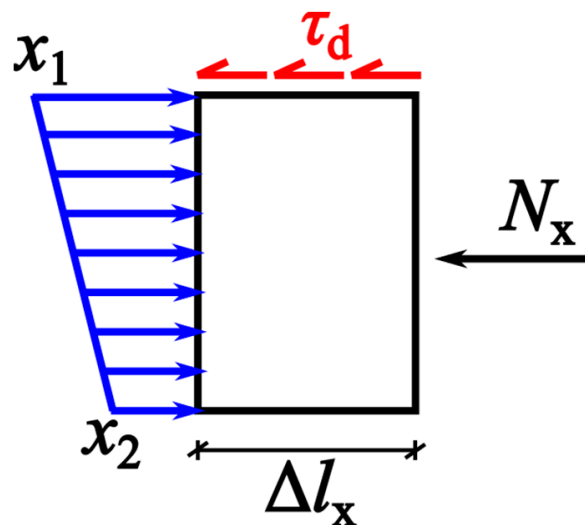where H_c is the height of the concrete core.

Figure 3. Segment Δl_x of the concrete core.

The cross-section ③ is located within the region of the intersection-line length $D_p/\sin\varphi$, while the shear stress τ_d is only applied to the top face of the steel tube, resulting in an eccentric force. In this case, the compressive stress on the top face of the steel tube can be calculated as follows:

$$\sigma_{s3} = \sigma_{s1} - \frac{\tau_d \Delta l_x}{T} + \frac{v \Delta d}{T} \tag{10}$$

where Δd is the distance to the right end of the intersection line in the x-direction.

The stresses on the top and bottom faces of the concrete core in the cross-section ③ can also be expressed by Equations (8) and (9), respectively. For the cross-section ④, the same stress in the concrete core can be found as that in the cross-section ③, while the stress on the top face of the steel tube is expressed by Equation (10). According to Figure 2, the maximum compressive stress on the steel tube is observed on the top face at a certain point, which is located in the region of the cross-sections ② and ④. The maximum compressive stress in the concrete core is also found at a certain point on the top face, where the shear-stress transfer is completed.

For the cross-section ⑤, the shear-stress transfer is completed, while the compressive stress on the top face of the steel tube is determined as follows:

$$\sigma_{s5} = \sigma_{s1} + \frac{\Delta V - \Delta V_c}{l_p T} \tag{11}$$

The compressive stresses on the top and bottom faces (σ_{c5t} and σ_{c5b}) of the concrete core for the cross-section ⑤ can be expressed by Equations (12) and (13), respectively.

$$\sigma_{c5t} = \sigma_{c1} + \frac{4\Delta V_c}{l_z H_c} \tag{12}$$

$$\sigma_{c5b} = \sigma_{c1} - \frac{2\Delta V_c}{l_z H_c} \tag{13}$$

Equations (1)–(13) can completely illustrate the stress distributions in the steel tube and concrete core in the region of the load transfer. To solve them, three unknown values, including the design value of the bond strength τ_d, the bond-transfer length l_x, and the bond-transfer circumference l_z, should be obtained. To address this, in the following section, the finite element model (FEM) is developed to determine the values of the three unknown values.

3.2. The FEM for the Joint between the Vertical Column and the CFST Arch Rib

A typical application of a deck CFST arch bridge in China, namely Shuangbao Bridge, was selected as the research object, and an overview of this bridge is introduced in Section 5. The FEM for the most critical joint between the vertical column and the CFST arch rib was developed using the commercial software ABAQUS, as presented in Figure 4. For the CFST arch rib, the circular hollow section had a diameter of 1400 mm and a thickness of 35 mm. For the vertical column, the steel-box section had dimensions of 2200 mm × 1000 mm, while the thicknesses were 16 mm and 22 mm in the x and z directions, respectively. To eliminate the stress concentration due to the Saint-Venant principle, the length of the arch rib was assumed to be 15 times the arch rib's diameter. Additionally, since the deformation of the vertical column was too small to be considered, it was employed as a rigid body with a height of 100 mm. As the load transfer was evaluated for the serviceability limit state, linear elastic material properties were assigned for both the steel and the concrete. The steel for the arch rib and vertical column had an elastic modulus E_s of 2.06×10^5 MPa and a Poisson's ratio of 0.31. The grade-C70 concrete specified in GB50010-2010 [44] was filled in the arch rib. The elastic modulus E_c and Poisson's ratio v_c were 3.7×10^4 MPa and 0.2, respectively. The vertical column, steel tube, and concrete core were simulated using C3D8 solid elements measuring 50 mm.
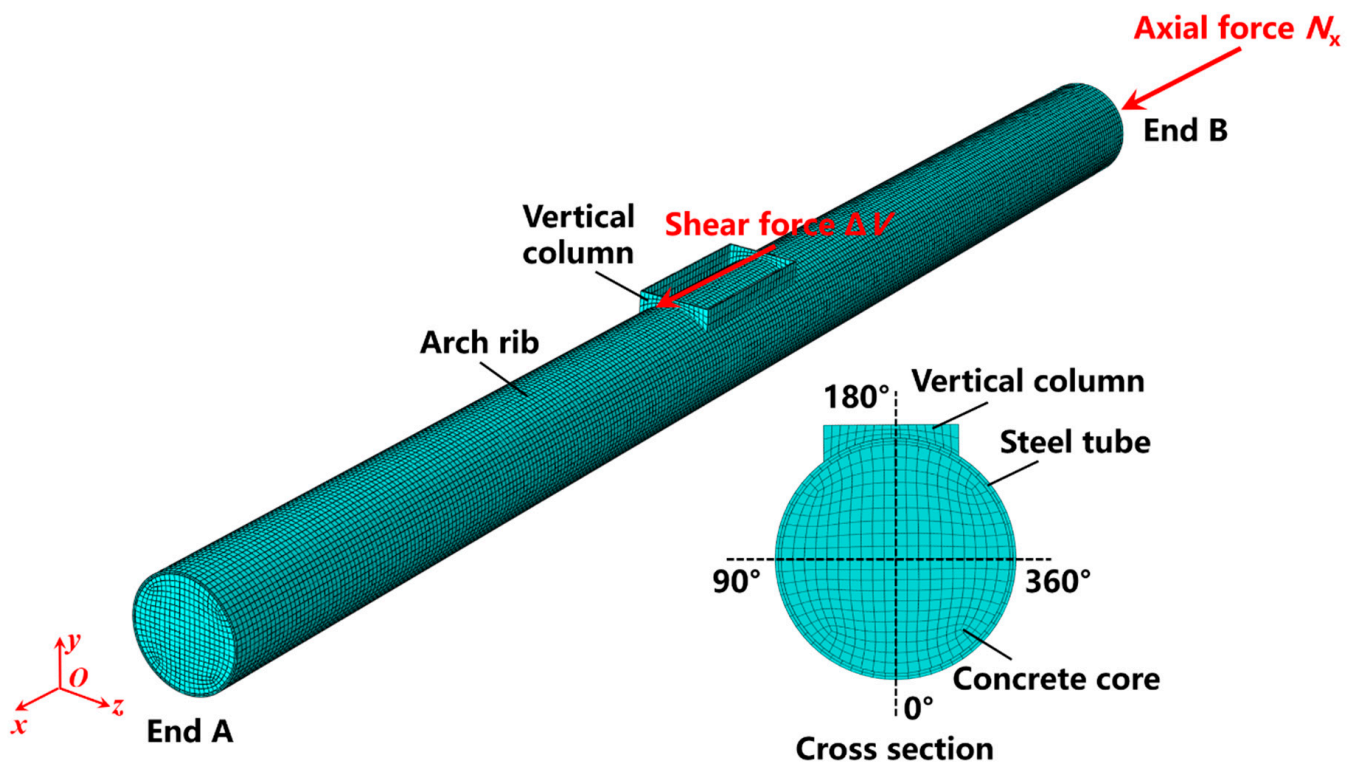

Figure 4. The FEM for the joint between the vertical column and CFST arch rib.

The bond at the steel–concrete interface is the key point in the accurate evaluation of the load-transfer mechanism. As shown in Figure 1, a relatively large difference was found between the bond stress–slip curves. To ensure the safety of the design, the most conservative curve of c (see Figure 1a) was assigned in the FEM. The surface-based cohesive contact with the traction-separation model available in the ABAQUS library was assigned, as illustrated in Figure 5. This model assumed a linear bond behavior with a constant shear modulus K prior to the bond strength τ_u, which was defined as stage I. Once the maximum bond stress was reached, this was regarded as the loss of the bond, while the damage criterion was met based on a user-defined damage-evolution law [13]. After the peak point, the curve decreased with a slope of α.
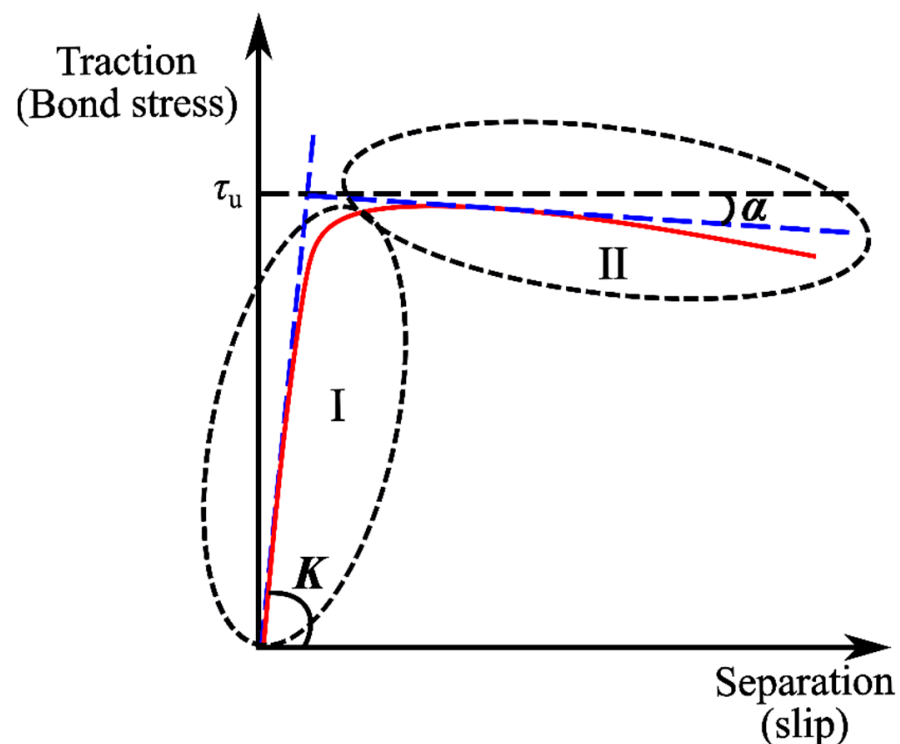

Figure 5. Traction-separation model.

For stage I, an elastic constitutive matrix, expressed in Equation (14), was adopted to illustrate the relationship between the normal (τ_n) and tangential (τ_s, τ_t) stresses (tractions) and the normal (δ_n) and tangential (δ_s, δ_t) slips at the steel–concrete interface. It was assumed that the bond stresses in three principal directions (see Figure 6) at the steel–concrete interface were uncoupled.

$$\begin{Bmatrix} \tau_n \\ \tau_s \\ \tau_t \end{Bmatrix} = \begin{bmatrix} k_{nn} & 0 & 0 \\ 0 & k_{ss} & 0 \\ 0 & 0 & k_{tt} \end{bmatrix} \begin{Bmatrix} \delta_n \\ \delta_s \\ \delta_t \end{Bmatrix} \tag{14}$$

where k_{nn}, k_{ss}, and k_{tt} are the initial stiffnesses in the n, s, and t directions, respectively, taken as $k_{nn} = k_{ss} = k_{tt} = 500$ N/mm^3, in accordance with [7].
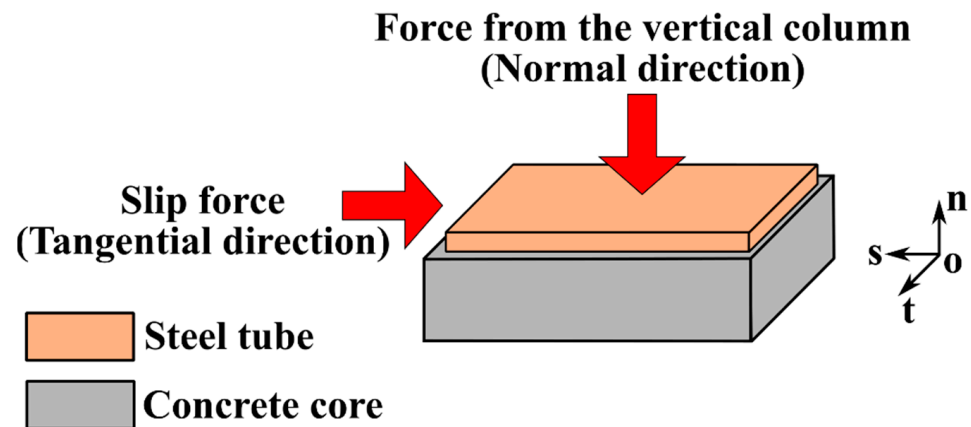
Figure 6. Definition of the directions at steel–concrete interface.

The loss of the bond was considered when the following maximum-stress criterion was reached:

$$\max\left\{\frac{\langle\tau_n\rangle}{\tau_n^o}, \frac{\tau_s}{\tau_s^o}, \frac{\tau_t}{\tau_t^o}\right\} = 1 \tag{15}$$

where τ_n^o is the bond strength in the normal direction, taken as 0.6 MPa, in accordance with [13]; τ_s^o and τ_t^o are the bond strengths in the two tangential directions, which can be conservatively taken as the minimum design value of the bond strength of 0.23 MPa specified in DBJ/T13-51-2010, as listed in Table 2.

The hard-contact behavior in ABAQUS was employed to the steel–concrete interface in the normal direction, which means that only separation from each other was allowed. For stage II, the value of α was taken as -0.014, as recommended by [13]. For the boundary conditions, fixed support ($Ux = Uy = Uz = URx = URy = URz = 0$) and pin support ($Uy = Uz = 0$) were employed to ends A and B, respectively. According to the numerical analysis of the whole bridge based on the software Midas Civil, the shear force at the joint (ΔV) of 2249 kN and the axial force on the CFST arch rib (N_x) of 24,888 kN under the most unfavorable loading conditions were derived and applied to the FEM in Figure 4. The FEM in this section was developed and validated according to [13].

3.3. Discussion on the FEM Results

Figure 7 shows the FEM results for the axial strain in the *x*-direction. It can be observed that the FEM results generally coincided with the analytical results, as shown in Figure 2. For the right side of the vertical column, the same calculated compressive strains of 300 $\mu\varepsilon$ were found for both the steel tube and the concrete core, which indicated that they worked together to resist the axial force, N_x. Furthermore, it was found that the bond-transfer length of 5.8 m was greater than the length of the intersection line, of 2.8 m, which demonstrated that the load transfer initiated at the location above the joint. Taking account of the bond stress, the compressive strain of the steel tube initially decreased and then increased, because the superposed compressive force was directly applied to the outer surface of the steel tube. For the location away from the joint, the compressive strain of the steel tube decreased and then tended to be a specific value. For the concrete core, the compressive strain increased due to the bond stress and then tended to be a specific value. It also should be noted that the region of the load introduction had symmetric distances above and below the joint. This conclusion can also be found in Figure 8.
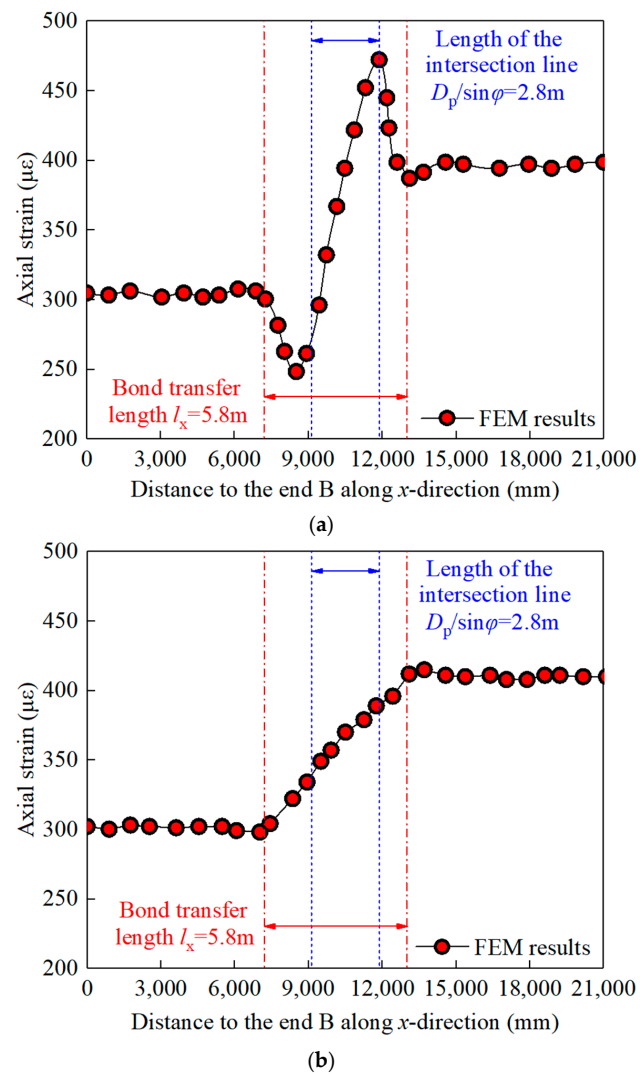
(a)

(b)

Figure 7. The FEM results for the axial strains in the *x*-direction: (**a**) steel tube; (**b**) concrete core.
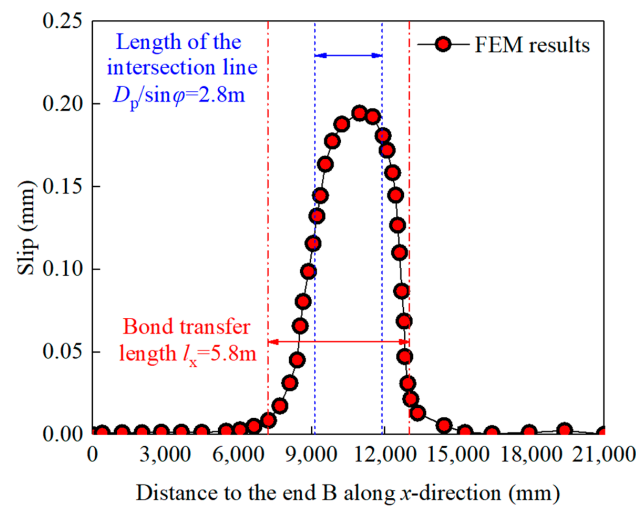

Figure 8. The FEM results for the longitudinal slip in the *x*-direction.

Figure 9 shows the FEM results for the steel–concrete interface slip along the middle section of the CFST arch rib, where the abscissa indicates the location on the cross-section of the CFST arch rib, as shown in Figure 4. It can be observed that the calculated bond-

transfer circumference was 1.1 m, which was approximately equal to the width of the intersection area. Therefore, the bond-transfer circumference l_z was assumed as the width of the intersection area.
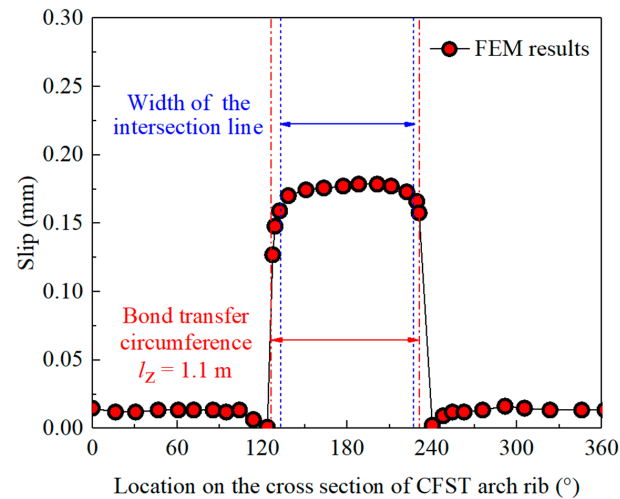

Figure 9. FEM results for the steel–concrete interface slip along the middle section of the CFST arch rib.

Through Equations (1)–(13), the force–equilibrium relationship for the load transfer in the typical joint in Shuangbao Bridge was obtained, as depicted in Figure 10. Based on the known parameters τ_d = 0.23 MPa and l_z = 1.1 m, the bond-transfer length can be calculated according to Equations (4)–(6).

$$l_x = \frac{\Delta V_c}{\tau_d l_z} = \frac{1405 \times 10^3}{0.23 \times 1.1 \times 10^3} = 5.6 \text{ m} \tag{16}$$
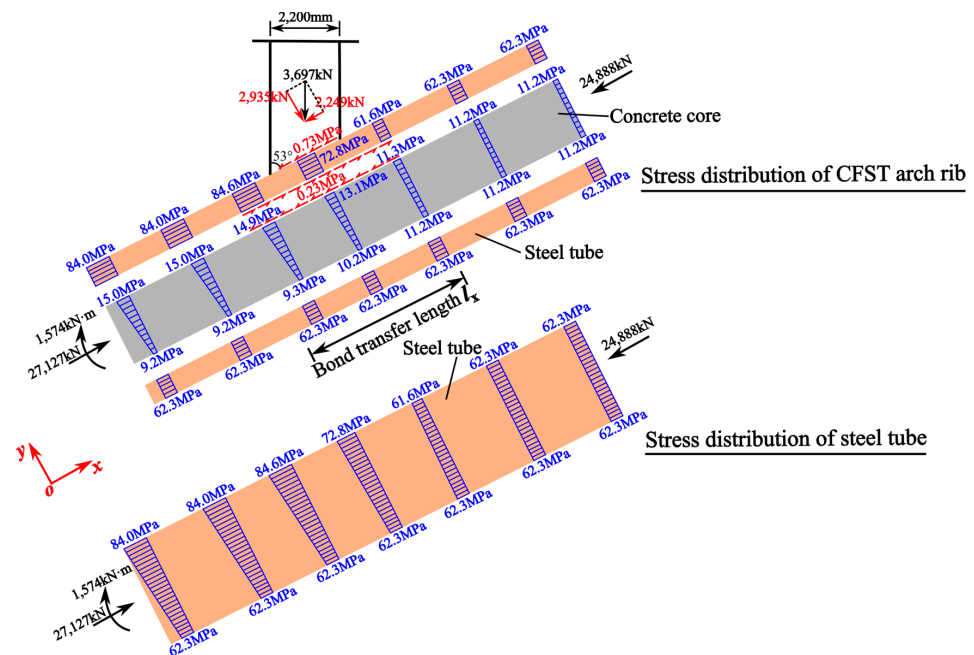

Figure 10. Force–equilibrium relationship for the load transfer in a typical joint in Shuangbao Bridge.

According to Equation (16), the theoretical bond-transfer length was 5.6 m, which essentially coincided with the FEM result of 5.8 m. This indicated that the load-transfer model in Figure 2 can effectively predict the practical situations.

4. Research on the Structural Details of Perfobond-Rib-Shear-Connectors in CFST Arch-Rib Joints

4.1. Geometrical Parameters of the Perfobond-Rib-Shear Connectors

Through properly attaching perfobond-rib-shear connectors to the inner surfaces of CFST arch ribs, the bond-transfer length can be reduced, and the bond behavior can be easily guaranteed. Figure 11 illustrates the geometrical parameters of the perfobond-rib-shear connectors, including the connector length l_p, the connector height h_p, the connector thickness t_p, the connector-hole diameter d_p, and the distance between the connector holes y_p. Figure 12 presents the arrangement of the perfobond-rib-shear connectors along the cross-section of the CFST arch ribs. Three types of arrangement along the cross-section should be addressed, according to the width of the intersection area, as follows: (a) the uniform arrangement along the whole cross-section, (b) the uniform arrangement along the upper half of the cross-section, and (c) the uniform arrangement along the width of the intersection area. Figure 13 depicts the arrangement of the perfobond-rib-shear connectors along the longitudinal section of the CFST arch ribs. Furthermore, two types of arrangement along the longitudinal section should be addressed, according to the region of the load introduction, as follows: (a) the symmetric arrangement above and below the joint and (b) the asymmetric arrangement above and below the joint.
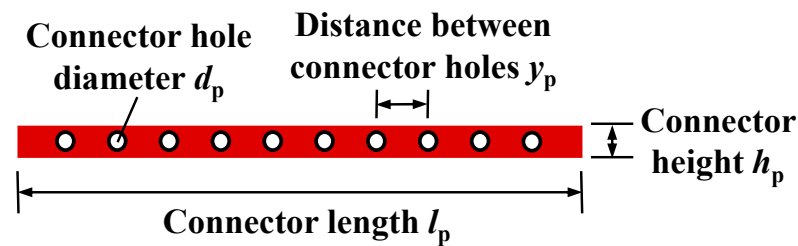

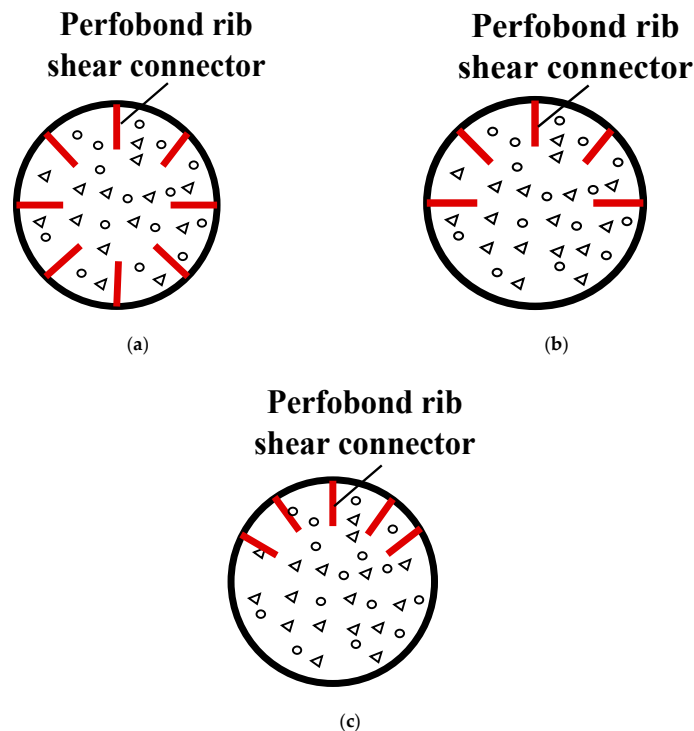**Figure 11.** Geometrical parameters of the perfobond-rib-shear connectors.

Figure 12. Arrangement of perfobond-rib-shear connectors along the cross-section of CFST arch ribs: (**a**) uniform arrangement along the whole cross-section; (**b**) uniform arrangement along the upper half of the cross-section; (**c**) uniform arrangement along the width of the intersection area.
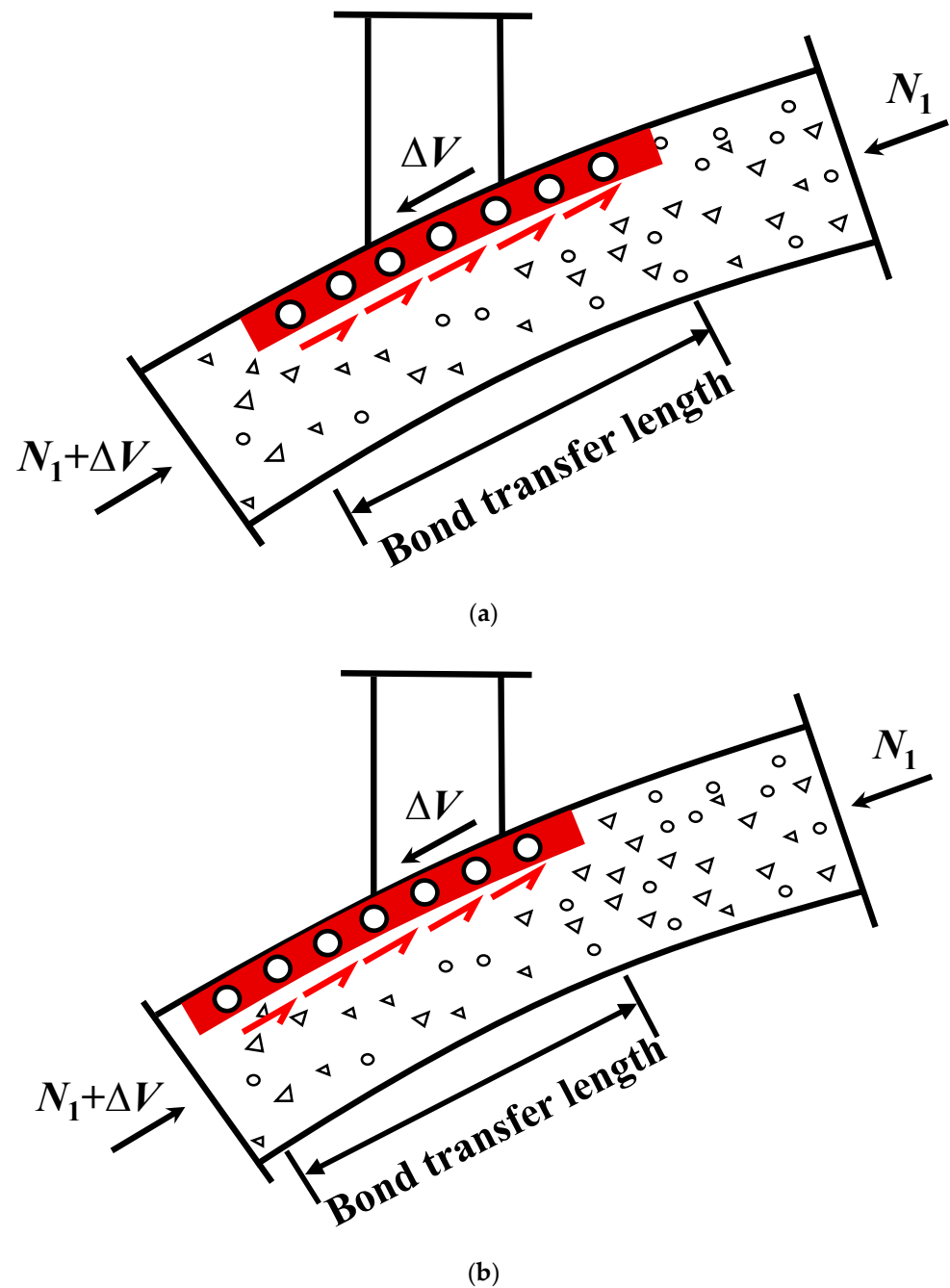
(**a**)

(**b**)

Figure 13. Arrangement of perfobond-rib-shear connectors along the longitudinal section of CFST arch ribs: (**a**) symmetric arrangement above and below the joint; (**b**) asymmetric arrangement above and below the joint.

4.2. Design Principles for the Parameters of Perfobond-Rib-Shear Connectors

Table 3 summarizes the design principles of the parameters of the perfobond-rib-shear connectors. Some of the parameter-design principles were influenced by a single factor; for example, the determination of the connector length was only influenced by the efficiency of the load transfer. However, the principles behind the other parameters were influenced by several factors, such as the connector height, which was itself comprehensively influenced by the efficiency of the load transfer, stiffening action, and constructability.

Table 3. Design principles for the parameters of perfobond-rib-shear connectors.

Factors	Dimensions of Perfobond-Rib-Shear Connectors					Arrangement Along the Cross-Section	Arrangement Along the Longitudinal Section
	Connector Length l_p	Connector Height h_p	Connector Thickness t_p	Connector-Hole Diameter d_p	Distance between Connector Holes y_p		
Efficiency of the load transfer	✓	✓		✓	✓		
Reduction due to the rib-hole group					✓		
Stiffening action		✓	✓				
Bond-transfer circumference						✓	
Region of the load introduction							✓
Constructability		✓				✓	

Similar to the steel–concrete interface, perfobond-rib-shear connectors can perform load transfer through the bond stress. It has been found that the typical bond stress–slip curve for a perfobond-rib-shear connector can be divided into three stages, which are the elastic, plastic, and hardening stages, while a continuous shear resistance can be provided after the bond strength is reached, leading to better ductility compared to the steel–concrete interface [45]. Liao [46] conducted push-out tests on perfobond-rib-shear connectors arranged in CFST columns and pointed out that the elastic stage of the bond stress–slip curve was too short, with a slip of less than 1 mm; furthermore, the shear modulus was in the range of 0.5–1.0 MPa, which was much larger than the shear modulus of the scenario without a perfobond rib shear connector of 0.165 MPa. Liao concluded that the perfobond-rib-shear connector reached the bond strength before the steel–concrete interface. Hence, it can be assumed that the shear force applied to the steel tube is transferred to the concrete core thoroughly by the perfobond-rib-shear connector. To date, many researchers have carried out push-out tests on perfobond-rib-shear connectors and proposed different equations to predict the shear capacity, as summarized in Table 4 [47–57]. In particular, some studies focused on the application of perfobond-rib-shear connectors in steel–concrete-composite bridges; thus, the contribution of transverse rebars in rib holes was taken into account. For perfobond-rib-shear connectors used in CFST arch ribs, only equations that do not consider the contribution of transverse rebars in rib holes can be used to predict the shear capacity, such as those proposed by Leonhardt et al. [47], Hosaka et al. [48], and Zhao et al. [49]. The conversion relationship between the cylinder's compressive concrete strength f_c' and the prism's compressive concrete strength f_c should be noted. The most conservative of the three equations described above, proposed by Leonhardt et al. [47], was adopted to predict the shear capacity of the perfobond-rib-shear connectors in this paper to address design-safety concerns. Additionally, the connector-hole diameter d_p, which is related to the connector height h_p, is an unknown value in the equation. As recommended by Cheng [58], an appropriate d_p should be taken as 0.5 h_p ~ 0.6 h_p to make full use of the material.

Table 4. Equations to predict the shear capacity of perfobond-rib-shear connectors.

Type	Reference	Equations	Applicable Conditions
Shear capacity per hole	Leonhardt et al. [47]	$V_{hole} = 1.4d_p^2 f_c'$	without transverse rebars in rib holes
	Hosaka et al. [48]	$V_P = 3.38\sqrt{t_p/d_p} \cdot d_p^2 f_c' - 39000$	without transverse rebars in rib holes
		$V_P = 1.45\left[\left(d_p^2 - d_{tr}^2\right)f_c' + d_s^2 f_y\right] - 26100$	with transverse rebars in rib holes
	Xue et al. [49]	$V_P = 2.936\pi\left(d_p^2 - d_{tr}^2\right)f_t + 0.289\pi d_{tr}^2 f_y$	with transverse rebars in rib holes
	Zhao et al. [50]	$V_P = 1.38d_p^2 f_c$	without transverse rebars in rib holes
		$V_P = 1.38\left(d_p^2 - d_{tr}^2\right)f_c + 1.24d_{tr}^2 f_y$	with transverse rebars in rib holes
Shear capacity per rib	Oguejiofor et al. [51,52]	$V_P = 0.590A_{cc}\sqrt{f_c'} + 2.871nd_p^2\sqrt{f_c'} + 1.233A_{tr}f_y$	with transverse rebars in rib holes
		$V_P = 4.50h_p t_p f_c' + 3.31nd_p^2\sqrt{f_c'} + 0.91A_{tr}f_y$	with transverse rebars in rib holes and replacement of splitting resistance of concrete with end-bearing resistance
	Veríssimo et al. [53]	$V_P = 4.04\left(h_p/b_c\right)h_p t_p f_c' + 2.37nd_p^2\sqrt{f_c'} + 0.16A_{cc}\sqrt{f_c'} + 31.85 \times 10^6\left(A_{tr}/A_{cc}\right)$	with transverse rebars in rib holes
	Medberry et al. [54]	$V_P = 0.747b_c h_f\sqrt{f_c'} + 0.413b_f L_c + 1.304nd_p^2\sqrt{f_c'} + 0.9A_{tr}f_y$	with transverse rebars in rib holes
	AI-Darzi et al. [55]	$V_P = 3.97nd_p^2\sqrt{f_c'} + 0.762h_p t_p f_c' - 7.59 \times 10^{-4}A_{tr}f_y + 255310$	with transverse rebars in rib holes
	Ahn et al. [56]	$V_P = 3.14h_p t_p f_c' + 2.98nd_p^2\sqrt{f_c'} + 1.21A_{tr}f_y$	single perfobond rib arranged with transverse rebars in rib holes
		$V_P = 2.76h_p t_p f_c' + 2.61nd_p^2\sqrt{f_c'} + 1.06A_{tr}f_y$	twin perfobond ribs arranged with transverse rebars in rib holes
	Zong et al. [57]	$V_P = 0.0029A_h\sqrt{E_c f_c'} + 0.75A_{tr}f_y$	with transverse rebars in rib holes

Note: V_{hole} is the shear capacity per hole; V_{PBL} is the shear capacity per connector; f_c' is the cylinder's compressive concrete strength; d_{tr} is the diameter of the transverse rebar; f_t is the tensile concrete strength; f_y is the yield strength of the transverse rebar; f_c is the prism's compressive concrete strength; A_{cc} is the longitudinal concrete shear area per connector; n is the connector-hole number; A_{tr} is the area of the transverse rebars in rib holes; b_c is the thickness of the concrete slab; h_f is the distance between the end of the perfobond rib and the end of the concrete slab; b_f is the width of the steel-beam flange; L_c is the contact length between the concrete slab and the steel-beam flange.

Regarding the shear strength per hole, V_{hole}, the connector length, l_p, can be determined based on the distance between the connector holes, y_p. The minimum connector length l_{pmin} should be determined to completely transfer the shear force applied to the concrete core ΔV_c, as follows:

$$l_{pmin} \geq ceil\left(\frac{\Delta V_c}{n_p V_{hole}}\right) \times y_p \tag{17}$$

where the *ceil*() function computes the nearest integer to a greater extent than the argument passed, and n_p is the number of perfobond-rib-shear connectors.

As pointed out by Tomii [59], the lateral deformation of the concrete core caught up with that of the steel tube when a certain longitudinal strain was reached, and this was considered the initiation of the confinement effect. At this stage, the concrete core was under triaxial compression, and the steel tube was under longitudinal compression and hoop tension. This stage was usually observed after the yield of the steel tube was in compliance with the von Mises yield criterion. As the force increased, the allowable hoop tension increased, and the allowable longitudinal compression continuously decreased, as shown in Figure 14. Under ideal conditions, point A was reached as the hoop stress reached the yield strength f_y and the longitudinal stress reached 0, as shown in Figure 15. At this point, the steel tube could not bear the longitudinal force; thus, the shear force ΔV in the longitudinal direction was transferred completely through the perfobond-rib-shear connector. The design value of the connector length l_{pd} is expressed as follows:

$$l_{pd} \geq ceil\left(\frac{\Delta V}{n_p V_{hole}}\right) \times y_p \tag{18}$$
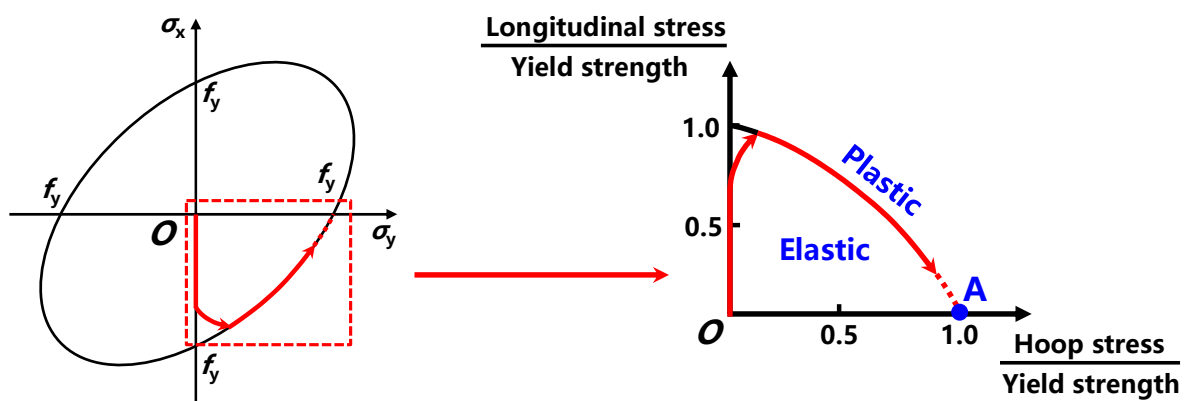

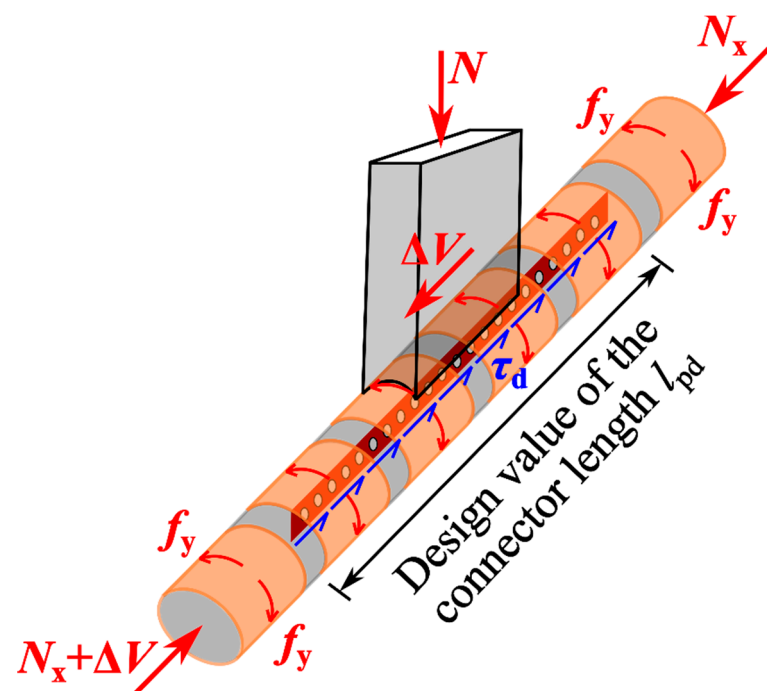**Figure 14.** Yield envelope and stress path of the steel tube.

Figure 15. Analytical model of the design value of the connector length.

According to the above analysis, the efficiency of the load transfer for the perfobond-rib-shear connector was related to the parameters l_p, h_p, d_p, and y_p. Among these, the determination of y_p was influenced by the reduction due to the rib-hole group, which meant that too small a distance between the connector holes would significantly reduce the shear strength. As recommended in [51,58], an appropriate y_p should be taken as 2–3 times the connector-hole diameter d_p.

In order to prevent the local buckling of the steel tube, the diameter-to-thickness ratio of CFST arch ribs should be in the range of 35–100, as recommended by GB 50923-2013. In addition, according to JTG/T D65-06-2015, the diameter-to-thickness ratio should be in the range of 24–90. Therefore, the stiffening action of the perfobond rib should be considered for a diameter-to-thickness ratio of greater than 90. According to the numerical analysis in Section 3.3, the bond-transfer circumference is equal to the width of the intersection line; thus, the arrangement of perfobond-rib-shear connectors along the cross-section of CFST arch ribs shown in Figure 12c should be selected. Additionally, the region of the load introduction had symmetric distances above and below the joint; thus, the arrangement of perfobond-rib-shear connectors along the longitudinal section of the CFST arch ribs in Figure 13a should be selected. Meanwhile, the circular steel tube is made by rolling, and therefore, a certain space is needed to weld the perfobond ribs to the inner surface of the steel tube. In practical applications, it is suggested to arrange the perfobond ribs in a circular steel tube with a diameter greater than 800 mm. For the use of more than one perfobond rib along the cross-section, a constructability analysis of the connector height and gap should be conducted.

4.3. Design Flow for the CFST Arch-Rib Joint with PerfobondRib Shear Connectors

Figure 16 presents the design flow for the CFST arch joint with perfobond-rib-shear connectors, including the selection of the geometrical parameters, the arrangement along the cross-section, and the longitudinal section of the CFST arch ribs. The details of the design flow are as follows:

- For the purpose of the design, the most critical joint is selected, and the corresponding shear force ΔV under the most unfavorable loading is determined.
- The diameter-to-thickness ratio is checked. If it is greater than 90, the stiffness of the perfobond ribs should be verified to prevent the local buckling of the steel tube; otherwise, no additional stiffeners should be set. According to the above principle, the connector height h_p and the connector thickness t_p are determined.
- The connector-hole diameter d_p should be taken as 0.5 h_p–0.6 h_p. Subsequently, the distance between the connector holes y_p should be taken as 2 d_p–3 d_p.
- The perfobond ribs should be uniformly arranged in the range of the bond-transfer circumference l_z along the cross-section. Hence, the number of perfobond ribs n_p and the gap between them s_p can be preliminarily determined. A constructability analysis should be conducted to adjust the parameters h_p, n_p, and s_p.
- The design value of the connector length l_{pd} is determined according to Equation (18), and the perfobond ribs should be arranged in the range of l_{pd}, with the symmetric distance above and below the joint along the longitudinal section.
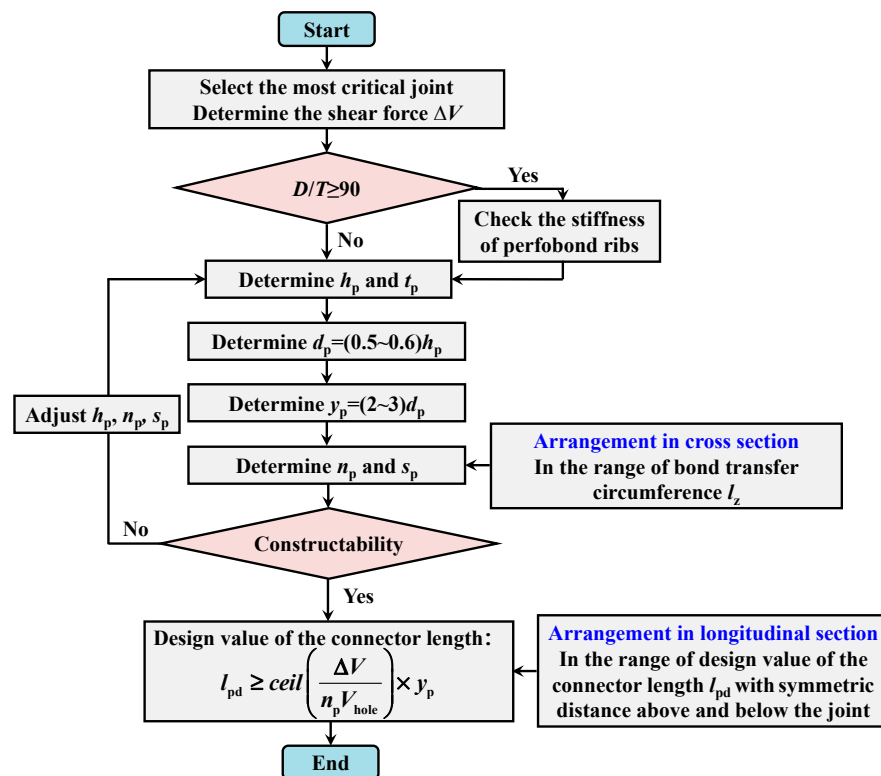
Figure 16. Design flow chart for the CFST arch rib joint with perfobond rib=shear connectors.

5. Optimization of the Joints in Shuangbao Bridge

5.1. Overview of Shuangbao Bridge

Shuangbao Bridge is a double-jointed deck CFST arch bridge with an overall span of 2×405 m. Figure 17 shows the elevation of one span of Shuangbao Bridge. This bridge has a calculated span of 380 m and a rise of 80 m, leading to a rise–span ratio of 1/4.75. The catenary curve was designed for the main trussed arch with an arch-axis coefficient of 1.55. The space truss was used for the arch rib with heights ranging from 11.0 m in the arch support to 6.5 m at the top of the arch.
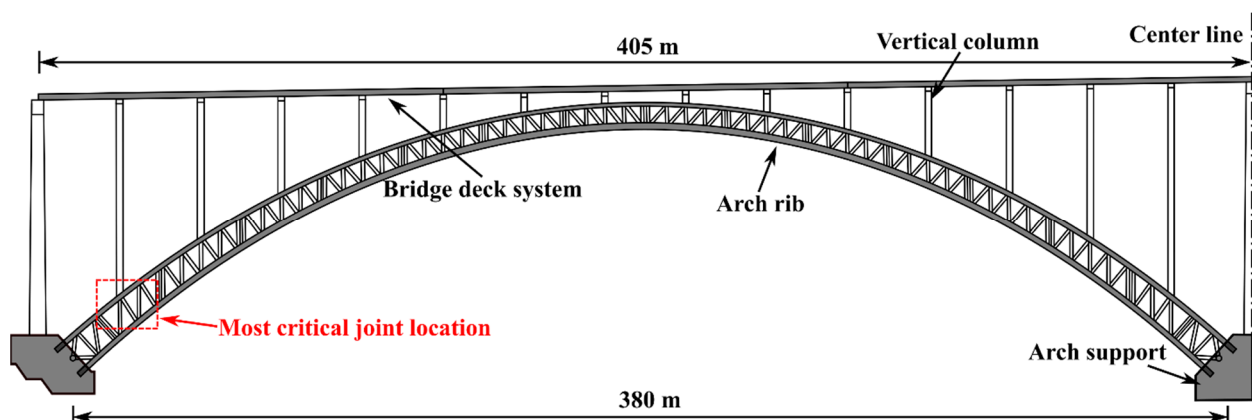
Figure 17. Elevation of the single span of Shuangbao Bridge.

The FEM of the whole bridge was developed using the commercial software Midas Civil, and the most critical joint was determined, as shown in Figure 17. Figure 18 illustrates the original design scheme of the joint between the vertical column and the CFST arch rib. The arch rib was designed as the truss structure, consisting of four CFST members. The chord has a diameter of 1400 mm and a thickness of 35 mm, while the vertical and diagonal

braces have diameters of 700 mm and thicknesses of 16 mm. A box section of 2200 mm ×
1000 mm was adopted for the vertical column. Furthermore, Q390D- and Q355D-grade
steels are used for the arch rib and vertical columns, respectively. The arch rib is filled
with concrete of grade C70. A steel inclined leg is arranged on the base of the vertical
columns, with a projected length l_b of 4823.8 mm. The intersection line between the two
braces and bottom chord (l_c) is 1593.8 mm. In order to enhance the bond strength, a series
of welded studs is arranged with a gap of 150 mm along the arch-rib axis for a total length
of l_b (l_c) + 600 mm. In addition, a total of 25 welded studs are arranged with an angular
spacing of 14.4° along the cross-section. For the most critical joint, 37 rows (n_s) of welded
studs, which number 925 in total, are arranged in the top chord over the layout length of
5400 mm. In total, 16 rows (n_s) of welded studs, which number 400 in total, are arranged in
the bottom chord over the layout length of 2250 mm. The dimensions of the welded studs
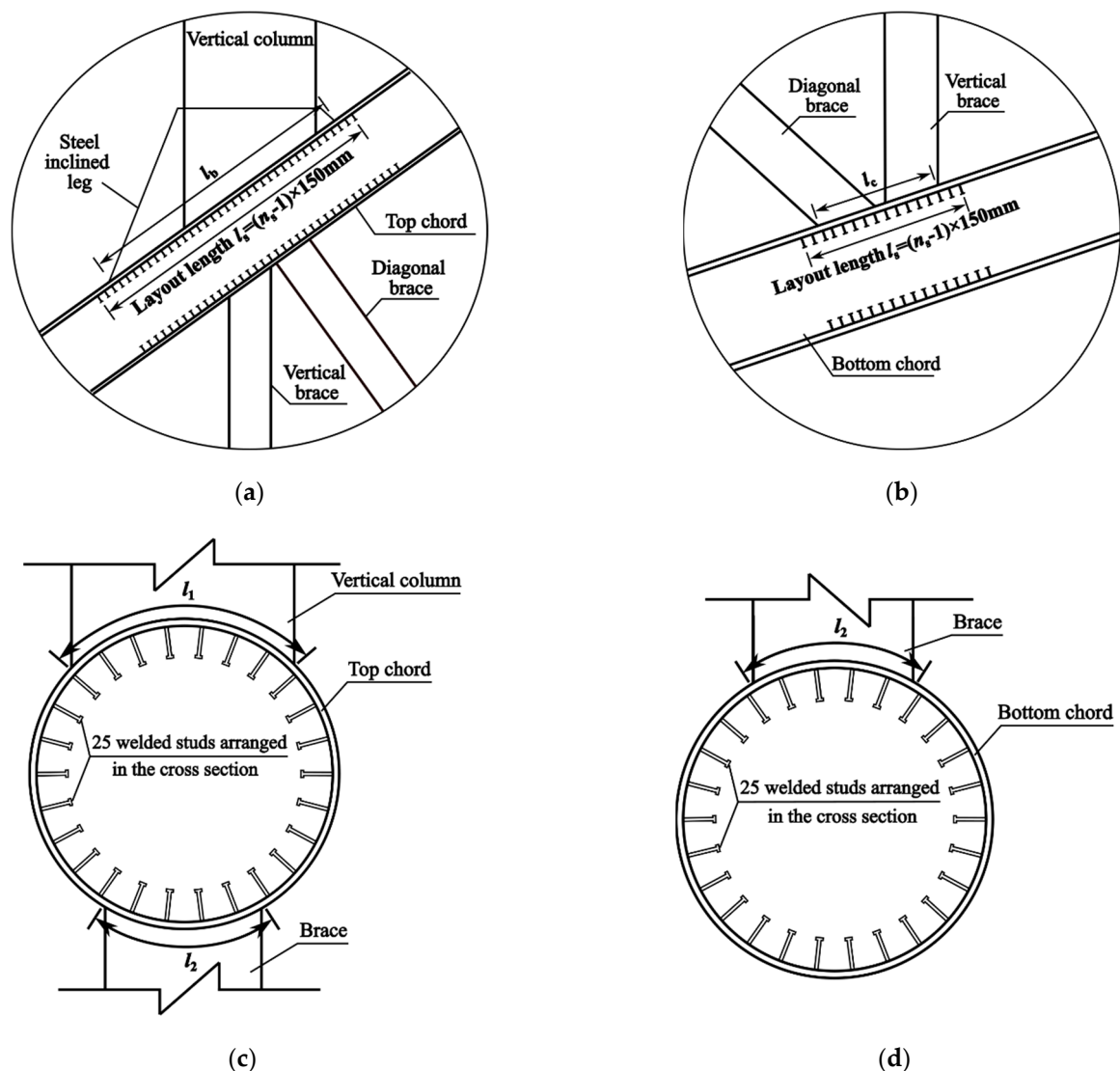are ML15 Φ16 × 150.

Figure 18. Original design scheme of the joint between the vertical column and CFST arch rib: (**a**) the
joint in the top chord of the CFST arch rib; (**b**) the joint in the bottom chord of the CFST arch rib;
(**c**) the cross-section of the top chord of the CFST arch rib; (**d**) the cross-section of the bottom chord of
the CFST arch rib.

5.2. Optimization of the Design of the Joint

Using the original design scheme of the joint, fabrication is a complicated process because of the use of such a large number of welded studs. On the other hand, the welded stud only works as a shear connector instead of a stiffener. For these reasons, it is suggested to optimize the design scheme of the joint in both the top and bottom chords of the CFST arch rib by replacing the welded studs with perfobond ribs.

According to the design flow chart (see Figure 16), it can be calculated that the diameter-to-thickness ratio at the most critical joint in Shuangbao Bridge is 40, which is smaller than 90. This indicates that there is no need to check the stiffness of the perfobond rib, and, thus, the height h_p and the thickness t_p are 200 mm and 16 mm, respectively. Hence, the connector-hole diameter d_p and the distance between the connector holes y_p are taken as 100 mm and 250 mm, which are 0.5 h_p and 2.5 d_p, respectively. For the joint in the top chord of the CFST arch rib, a total of five perfobond ribs were designed to be uniformly arranged on the top face of the steel tube over the length of the intersection line (l_1 = 1114 mm) at an angular spacing of 23.5°, while a total of three perfobond ribs were designed to be uniformly arranged on the bottom face of the steel tube along the length of the intersection line (l_2 = 733 mm) at an angular spacing of 23.5°. Furthermore, the perfobond rib was arranged on the top and bottom faces of the bottom chord in the same way. A constructability analysis was conducted based on the optimized design scheme, which showed the minimum gap between the perfobond ribs in the cross-section is 191 mm. This is greater than the original design scheme of 129 mm, indicating sufficient constructability.

According to Equation (18), the design value of the connector length l_{pd} for the top face of the top chord is:

$$l_{pd} \geq ceil\left(\frac{\Delta V}{n_p V_{hole}}\right) \times y_p = ceil\left(\frac{2249 \times 1000}{5 \times 1.4 \times 30.5 \times 100^2}\right) \times 250 = 500 \text{ mm} \quad (19)$$

The design values of the connector length l_{pd} for the bottom face of the top chord and the top and bottom faces of the bottom chord are:

$$l_{pd} \geq ceil\left(\frac{\Delta V}{n_p V_{hole}}\right) \times y_p = ceil\left(\frac{2249 \times 1000}{3 \times 1.4 \times 30.5 \times 100^2}\right) \times 250 = 500 \text{ mm} \quad (20)$$

where the concrete strength is taken as the design value of the axial compressive strength of 30.5 MPa.

In Section 3.3, it was demonstrated that the bond-transfer length was 5600 mm for the top face of the top chord. According to the result of Equation (18), the bond-transfer length was only 500 mm after arranging the perfobond rib, as shown in Figure 19. For the top face of the top chord, the layout length of the perfobond rib was taken as 5250 mm in consideration of the inclined steel leg. For the other faces, the layout length of the perfobond rib was taken as 2000 mm.

5.3. Comparison between the Original and Optimized Design Schemes of the Joint

Table 5 lists the comparison between the original and optimized design schemes of the joint. According to the FEM results in Section 3.3, the bond-transfer circumference was equal to the width of the intersection line; thus, it was deemed that only welded studs arranged in this region can work. The numbers of welded studs along l_1 and l_2 (see Figure 18) are listed in Table 5. As recommended by JTG/T D64-01-2015 [60], the shear capacity of the single welded stud can be determined by Equation (21). Additionally, some studies have indicated that a reduction of 0.67–0.98 should be considered for the shear capacity due to the welded studs' group arrangement. In this paper, a conservative reduction value of 0.67 is taken.
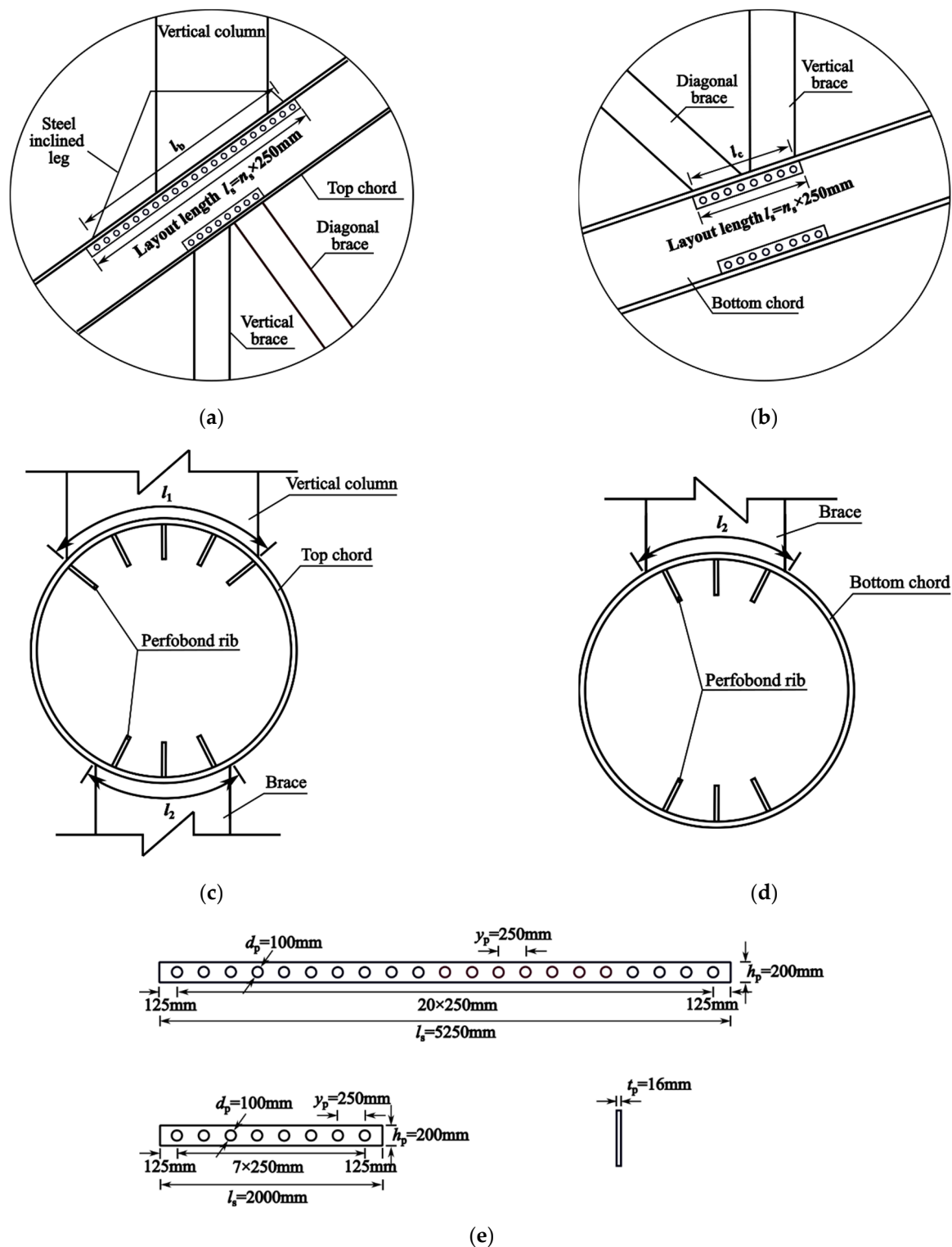
Figure 19. Optimized design scheme of the joint between the vertical column and CFST arch rib: (**a**) the joint in the top chord of the CFST arch rib; (**b**) the joint in the bottom chord of the CFST arch rib; (**c**) the cross-section of the top chord of the CFST arch rib; (**d**) the cross-section of the bottom chord of the CFST arch rib; (**e**) dimensions of the perfobond rib.

$$V_{\text{stud}} = \min\left\{ 0.43 A_{\text{stud}} \sqrt{E_c f_{\text{cd}}}, 0.7 A_{\text{stud}} f_{\text{su}} \right\} \tag{21}$$

where V_{stud} is the shear capacity of the single welded stud; A_{stud} is the area of the welded stud rod; f_{cd} is the design value of the axial compressive strength for concrete; f_{su} is the tensile strength of the welded stud.

Table 5. Comparison between the original and optimized design schemes of the joints.

Location	Welded Studs				Perfobond Ribs				Comparisons		
	Number	Layout Length l_S (mm)	Shear Resistance vs. (kN)	Steel Consumption Q_S (ton)	Number	Layout Length l_P (mm)	Shear Resistance V_P (kN)	Steel Consumption Q_P (ton)	l_P/l_S	V_P/V_S	Q_P/Q_S
① Top face of the top chord	296	5400	11,166		5	5250	44,835		0.97	4.02	
② Bottom face of the top chord	148	5400	5582		3	2000	10,248		0.37	1.84	
③ Top face of the bottom chord	96	2250	3621	0.17	3	2000	10,248	1.10	0.89	2.83	6.47
④ Bottom face of the bottom chord	96	2250	3621		3	2000	10,248		0.89	2.83	

As shown in Table 5, the numbers of welded studs arranged at locations ①–④ were 296, 148, 96, and 96, respectively. Correspondingly, the numbers of perfobond ribs arranged at locations ①–④ were 5, 3, 3, and 3, respectively. The layout lengths for these locations in the original design scheme are 5400 mm, 5400 mm, 2250 mm, and 2250 mm, respectively. The layout lengths for these locations in the optimized design scheme are 5250 mm, 2000 mm, 2000 mm, and 2000 mm. It was found that the layout lengths of the perfobond ribs were similar with those of the welded studs, except at location ②. On this basis, a comparison between the steel consumption and shear resistance was made. The shear-resistance ratios of the perfobond ribs (V_P) to the welded studs (V_S) were 4.02, 1.84, 2.83, and 2.83 for locations ①–④, respectively, while the steel consumptions of the perfobond ribs (Q_P) and welded studs (Q_S) were 1.10 tons and 0.17 tons, respectively. Although an increase in the steel consumption of the perfobond ribs compared to that of the welded studs was found, a significant increase of 1.84~4.02 was also observed for the shear resistance of the perfobond ribs compared to the welded studs. It can be concluded that the optimized design scheme had the most efficient load-transfer efficiency. Furthermore, the perfobond ribs were more convenient for the fabrication than the welded studs.

6. Conclusions

This paper studied the mechanism of the load transfer for the novel joints between vertical columns and CFST arch ribs with perfobond-rib-shear connectors. The typical parameters, including the geometric dimensions of the perfobond rib and the arrangements of the perfobond rib along the cross-section and longitudinal section of the arch rib, were evaluated. A design flow for the CFST arch-rib joint with perfobond-rib-shear connectors was proposed. The optimization of the joints in Shuangbao Bridge by replacing welded studs with perfobond ribs was conducted. Based on these investigations, the following conclusions may be drawn:

1. The force–equilibrium relationship for the load transfer at the joint between the vertical columns and the CFST arch ribs was determined. In particular, the design value of the bond strength was taken as 0.23 MPa, as specified in DBJ/T13-51-2010. The shear stress applied to the top face of the steel tube was transferred to the top face of the concrete core through the steel–concrete interface with an arc area. The arc area of the contact surface had symmetric distances above and below the joint in the

x-direction. Additionally, the bond-transfer circumference was equal to the width of the intersection area.

2. For the geometric dimensions of the perfobond ribs, the following key factors should be considered: the efficiency of the load transfer, reduction due to the rib holes group, stiffening action, bond-transfer circumference, region of the load transfer, and constructability. The perfobond ribs should be uniformly arranged over the width of the intersection area along the cross-section and symmetrically arranged above and below the joint along the longitudinal section.

3. Significant increases in shear resistance, by factors of 1.84–4.02, were found for the perfobond ribs compared to the welded studs. It can be concluded that the optimized design scheme had the most efficient load transfer. Furthermore, the perfobond rib was more convenient for the fabrication than the welded stud.

Notations

A_c	cross-sectional area of the concrete core;
A_{cc}	longitudinal concrete shear area per connector;
A_p	Top-face area of the steel tube within the length of the intersection line, between vertical column and CFST arch rib;
A_T	area of the contact surface;
A_{tr}	area of the transverse rebars in rib holes;
A_s	cross-sectional area of the steel tube;
A_{stud}	area of the welded stud rod;
b_c	thickness of the concrete slab;
b_f	width of the steel-beam flange;
D	diameter of the steel tube;
D_p	height of the cross-section of the vertical column;
d_p	connector-hole diameter;
d_{tr}	diameter of the transverse rebar;
Δd	distance to the right end of the intersection line in the x-direction;
E_c	elastic modulus of the concrete;
E_s	elastic modulus of the steel;
f_c	prism compressive concrete strength;
f_c'	cylinder compressive concrete strength;
f_{cd}	design value of the axial compressive strength for concrete;
f_t	tensile concrete strength;
f_{su}	tensile strength of the welded stud;
f_y	yield of the transverse rebar;
H	height of the concrete core;
h_f	distance between the end of the perfobond rib and the end of the concrete slab;
h_p	connector height;

K	shear modulus;
k_{nn}, k_{ss}, k_{tt}	initial stiffnesses in the n, s, and t directions, respectively;
L	length of the CFST column;
L_c	contact length between the concrete slab and the steel-beam flange;
l_b	projected length of the steel inclined leg arranged at the base of the vertical column;
l_c	the length of the intersection line between two braces and bottom chord;
l_p	connector length;
l_{pmin}	minimum connector length;
l_{pd}	design value of the connector length;
l_P	layout lengths of perfobond ribs;
l_S	layout lengths of welded studs;
l_w	arc width of the cross-section of the vertical column;
l_x	Bond-transfer length;
Δl_x	distance of an assumed segment;
l_z	bond-transfer circumference;
N	vertical load applied to vertical column;
N_x	axial force applied to the CFST arch rib transferred from the vertical column;
ΔN	vertical force component of N;
n	connector-hole number;
n_p	perfobond-rib-shear-connector number;
n_s	the number of the row of welded studs;
Q_P	steel consumption of perfobond ribs;
Q_S	steel consumption of welded studs;
s_p	gap between perfobond-rib-shear connectors;
T	thickness of the steel tube;
t_p	connector thickness;
V_{hole}	shear capacity per hole;
V_P	shear resistance of perfobond ribs;
V_{PBL}	shear capacity per connector;
V_S	shear resistance of welded studs;
V_{stud}	shear capacity of the single welded stud;
ΔV	Horizontal-force component of N;
ΔV_c	horizontal force applied to the concrete;
v	shear stress on the top face of the steel tube;
v_c	Poisson's ratio of the concrete;
v_s	Poisson's ratio of the steel;
y_p	distance between connector holes;
σ_{c1}	compressive stress on the concrete core in cross-section ①;
σ_{c2t}	compressive stress on the top face of the concrete core in cross-section ②;
σ_{c2b}	compressive stress on the bottom face of the concrete core in cross-section ②;
σ_{c5t}	compressive stress on the top face of the concrete core in cross-section ⑤;
σ_{c5b}	compressive stress on the bottom face of the concrete core in cross-section ⑤;
σ_{s1}	compressive stress on the steel tube in cross-section ①;
σ_{s3}	compressive stress on the steel tube in cross-section ③;
σ_{s5}	compressive stress on the steel tube in cross-section ⑤;
α	slope for the traction-separation model after the peak point;
δ_n	normal slip;

δs, δt	tangential slip;
τd	design value of the bond strength;
τu	bond strength;
τn	normal traction;
τs, τt	tangential traction;
τno	bond strength in the normal direction;
τso, τto	bond strength in two tangential directions;
φ	angle between the vertical column and CFST arch rib.

References

1. Zheng, J.; Wang, J. Concrete-filled steel tube arch bridges in China. *Engineering* **2018**, *4*, 143–155. [CrossRef]
2. Chen, B.; Wang, T.L. Overview of concrete filled steel tube arch bridges in China. *Pract. Period. Struct. Des. Constr.* **2009**, *14*, 70–80. [CrossRef]
3. Zhang, W.; Wang, R.; Zhao, H.; Lam, D.; Chen, P. Axial-load response of CFST stub columns with external stainless steel and recycled aggregate concrete: Testing, mechanism analysis and design. *Eng. Struct.* **2022**, *256*, 113968. [CrossRef]
4. Lai, M.H.; Song, W.; Ou, X.L.; Chen, M.T.; Wang, Q.; Ho, J. A path dependent stress-strain model for concrete-filled-steel-tube column. *Eng. Struct.* **2020**, *211*, 110312. [CrossRef]
5. Gao, W.; Zhao, J.; Fan, J.; You, H.; Wang, Z. A theoretical model for predicting mechanical properties of circular concrete-filled steel tube short columns. *Structures* **2022**, *45*, 572–585. [CrossRef]
6. Lai, Z.; Jiang, H.; Cai, Y. A new design equation to estimate the axial compressive strength of circular concrete-filled steel tubular stub columns. *Structures* **2022**, *46*, 1043–1054. [CrossRef]
7. Wang, F.; Xie, W.; Li, B.; Han, L. Experimental study and design of bond behavior in concrete-filled steel tubes (CFST). *Eng. Struct.* **2022**, *268*, 114750. [CrossRef]
8. Dong, H.; Chen, X.; Cao, W.; Zhao, Y. Bond-slip behavior of large high-strength concrete-filled circular steel tubes with different constructions. *J. Constr. Steel Res.* **2020**, *167*, 105951. [CrossRef]
9. Naghipour, M.; Khalili, A.; Hasani, S.M.R.; Nematzadeh, M. Experimental investigation of natural bond behavior in circular CFTs. *Steel Compos. Struct.* **2022**, *42*, 191–207. [CrossRef]
10. Lin, Y.; Zhao, Z.; Gao, X.; Wang, Z.; Qu, S. Behavior of concrete-filled U-shaped steel beam to CFSST column connections. *Buildings* **2023**, *13*, 517. [CrossRef]
11. Luo, J.; Gao, S.; Zhang, Y.; Guo, X.; Chen, S.; Ding, F. Load-transfer mechanism of distribution beams in giant rectangular concrete-filled steel tubular columns. *J. Constr. Steel Res.* **2022**, *197*, 107487. [CrossRef]
12. Ami, M.; Zahrai, S.M. Compressive behavior and design of octagonal rubberized concrete-filled double steel tubular stub columns stiffened by headed studs. *Structures* **2022**, *42*, 104–124. [CrossRef]
13. Mollazadeh, M.H.; Wang, Y.C. New insights into the mechanism of load introduction into concrete-filled steel tubular column through shear connection. *Eng. Struct.* **2014**, *75*, 139–151. [CrossRef]
14. Mollazadeh, M.H.; Wang, Y.C. New mechanism of load introduction into concrete-filled steel tubular columns. *J. Struct. Eng.* **2016**, *142*, 4016016. [CrossRef]
15. Yan, X.; Shi, S.; Liu, X.; Mao, H. Numerical analysis of mechanical behavior of self-centering joint between CFDST column and RC beam. *Buildings* **2023**, *13*, 135. [CrossRef]
16. Ramírez Ortiz, C.; Gutierrez Amador, A.D.; Ramírez Duque, J.L. Numerical analysis of the seismic behavior of a steel beam-to-concrete-filled steel tubular column connection using external diaphragms. *Buildings* **2022**, *12*, 1217. [CrossRef]
17. Debnath, P.P.; Xu, F.; Chan, T. Load transfer mechanism in concrete-filled steel tubular columns: Developments, challenges and opportunities. *J. Constr. Steel Res.* **2023**, *203*, 107781. [CrossRef]
18. Song, S.; Xu, F.; Chen, J.; Wang, Y. Mechanism of load introduction and transfer within steel-encased concrete-filled steel tube connections. *J. Constr. Steel Res.* **2023**, *203*, 107818. [CrossRef]
19. Chen, H.; Nie, X.; Gan, S.; Zhao, Y.; Qiu, H. Interfacial imperfection detection for steel-concrete composite structures using NDT techniques: A state-of-the-art review. *Eng. Struct.* **2021**, *245*, 112778. [CrossRef]
20. Gong, S.; Feng, X.; Zhang, G.; Ansari, F. Distributed detection of internal cavities in concrete-filled steel tube arch bridge elements. *Struct. Health Monit.* **2023**, *22*, 657–671. [CrossRef]
21. Zhou, X.; Liu, Y.; Jiang, L.; Zhang, N. Review on mechanical behavior research of concrete filled rectangular hollow section tube stiffened with PBL. *China J. Highw. Transp.* **2017**, *30*, 45–62. (In Chinese)
22. Liu, Y.; Xiong, Z.; Feng, Y.; Jiang, L. Concrete-filled rectangular hollow section X joint with Perfobond Leister rib structural performance study: Ultimate and fatigue experimental Investigation. *Steel Compos. Struct.* **2017**, *24*, 455–465. [CrossRef]
23. Jiang, L.; Liu, Y.; Fam, A.; Liu, J.; Liu, B. Stress concentration factor parametric formulae for concrete-filled rectangular hollow section K-joints with perfobond ribs. *J. Constr. Steel Res.* **2019**, *160*, 579–597. [CrossRef]
24. Jiang, L.; Liu, Y.; Fam, A. Stress concentration factors in concrete-filled square hollow section joints with perfobond ribs. *Eng. Struct.* **2019**, *181*, 165–180. [CrossRef]

25. Jiang, L.; Liu, Y.; Fam, A.; Wang, K. Fatigue behaviour of non-integral Y-joint of concrete-filled rectangular hollow section continuous chord stiffened with perfobond ribs. *Eng. Struct.* **2019**, *191*, 611–624. [CrossRef]

26. Jiang, L.; Liu, Y.; Fam, A.; Liu, B.; Long, X. Fatigue behavior of integral built-up box Y-joints between concrete-filled chords with perfobond ribs and hollow braces. *J. Struct. Eng.* **2020**, *146*, 4019218. [CrossRef]

27. Jiang, L.; Liu, Y.; Fam, A.; Liu, B.; Pu, B.; Zhao, R. Experimental and numerical analyses on stress concentration factors of concrete-filled welded integral K-joints in steel truss bridges. *Thin Wall. Struct.* **2023**, *183*, 110347. [CrossRef]

28. Cheng, G.; Liu, Y.; Li, H.; Zhang, N.; Su, J. Testing and analysis of concrete-filled square hollow section stub columns with perfobond leister rib. *Teh. Vjesn.* **2019**, *26*, 1081–1090. [CrossRef]

29. Mollazadeh, M.H. *Load Introduction into Concrete-Filled Steel Tubular Columns*; The University of Manchester: Manchester, UK, 2015.

30. Virdi, K.S.; Dowling, P.J. Bond strength in concrete filled steel tubes. *IABSE Proc.* **1980**, *4*, 125–139.

31. Roeder, C.W.; Cameron, B.; Brown, C.B. Composite action in concrete filled tubes. *J. Struct. Eng.* **1999**, *125*, 477–484. [CrossRef]

32. Aly, T.; Elchalakani, M.; Thayalan, P.; Patnaikuni, I. Incremental collapse threshold for pushout resistance of circular concrete filled steel tubular columns. *J. Constr. Steel Res.* **2010**, *66*, 11–18. [CrossRef]

33. Tao, Z.; Song, T.; Uy, B.; Han, L. Bond behavior in concrete-filled steel tubes. *J. Constr. Steel Res.* **2016**, *120*, 81–93. [CrossRef]

34. Xu, C.; Chengkui, H.; Decheng, J.; Yuancheng, S. Push-out test of pre-stressing concrete filled circular steel tube columns by means of expansive cement. *Constr. Build. Mater.* **2009**, *23*, 491–497. [CrossRef]

35. Xue, L.; Cai, S. Bond strength at the interface of concrete-filled steel tube columns, Part I. *Build. Sci.* **1996**, *12*, 22–28. (In Chinese)

36. Xue, L.; Cai, S. Bond strength at the interface of concrete-filled steel tube columns, Part II. *Build. Sci.* **1996**, *12*, 19–23. (In Chinese)

37. Liu, Y.; Chi, J. Push-out test on shear bond strength of CFST. *Ind. Constr.* **2006**, *36*, 78–80. (In Chinese)

38. Liu, Y.; Liu, J.; Chi, J. Shear bond behaviors at interface of concrete-filled steel tube. *J. Guangxi Univ.* **2010**, *35*, 17–23. (In Chinese)

39. *DBJ/T13-51-2010*; Technical Specification for Concrete-Filled Steel Tubular Structures. Department of Housing and Urban-Rural in Fujian Province: Fuzhou, China, 2010.

40. *BS EN 1994-1-1*; Eurocode 4: Design of Composite Steel and Concrete Structures—Part 1-1: General Rules and Rules for Buildings. British Standards Institution: London, UK, 2004.

41. *BS 5400-5: 2005*; Steel, Concrete and Composite Bridges—Part 5: Code of Practice for the Design of Composite Bridges. British Standards Institution: London, UK, 2005.

42. *AS 5100.6-2004*; Bridge Design—Part 6: Steel and Composite Construction. Standards Australia International Ltd.: Sydney, Australia, 2004.

43. *ANSI-AISC 360-05*; Specification for Structural Steel Building. American Institute of Steel Construction: Chicago, IL, USA, 2010.

44. *GB50010-2010*; Code for Design of Concrete Structures. China Architecture & Building Press: Beijing, China, 2010.

45. Vianna, J.d.C.; de Andrade, S.; Vellasco, P.C.G.D.; Costa-Neves, L.F. Experimental study of perfobond shear connectors in composite construction. *J. Constr. Steel Res.* **2013**, *81*, 62–75. [CrossRef]

46. Liao, C. *Experimental Study on the Ultimate Shear Capacity of Grouped Stud Connectors in Continuous Composite Steel-Concrete Girder Bridge*; Tongji University: Shanghai, China, 2007. (In Chinese)

47. Leonhardt, F.; Andrae, W.; Andrae, H.; Harre, W. New, improved bonding means for composite load bearing structures with high fatigue strength. *Beton-Und Stahlbetonbau* **1987**, *82*, 325–331. [CrossRef]

48. Hosaka, T.; MItsugi, K.; Hiragi, H.; Ushijima, H. Study on shear strength and design method of perfobond strip. *Jpn. J. Struct. Eng.* **2002**, *48*, 1265–1272.

49. Xue, W.; Dai, Y.; Zhou, L.; Lu, Y. Experimental studies on shear behavior of perfobond connectors. *J. Build. Struct.* **2009**, *30*, 103–111. (In Chinese)

50. Zhao, C.; Liu, Y. Experimental study of shear capacity of perfobond connector. *Eng. Mech.* **2012**, *29*, 349–354. (In Chinese)

51. Oguejiofor, E.C.; Hosain, M.U. A parametric study of perfobond rib shear connectors. *Can. J. Civ. Eng.* **1994**, *21*, 614–625. [CrossRef]

52. Oguejiofor, E.C.; Hosain, M.U. Numerical analysis of push-out specimens with perfobond rib connectors. *Comput. Struct.* **1997**, *62*, 617–624. [CrossRef]

53. Veríssimo, G.S.; Paes, J.R.; Valente, I.; Cruz, P.J.; Fakury, R.H. Design and experimental analysis of a new shear connector for steel and concrete composite structures. In Proceedings of the 3rd International Conference on Bridge Maintenance, Safety, Management, Life-cycle Performance and Cost, Porto, Portugal, 16–19 July 2006; Taylor & Francis: London, UK, 2006.

54. Medberry, S.B.; Shahrooz, B.M. Perfobond shear connector for composite construction. *Eng. J.* **2002**, *39*, 2–12.

55. Al-Darzi, S.Y.K.; Chen, A.R.; Liu, Y.Q. Finite element simulation and parametric studies of perfobond rib connector. *Am. J. Appl. Sci.* **2007**, *4*, 122–127. [CrossRef]

56. Ahn, J.H.; Lee, C.G.; Won, J.H.; Kim, S.H. Shear resistance of the perfobond-rib shear connector depending on concrete strength and rib arrangement. *J. Constr. Steel Res.* **2010**, *66*, 1295–1307. [CrossRef]

57. Zong, Z.; Che, H. Experimental study of shear connector under static and fatigue loading. *J. Fuzhou Univ.* **1999**, *27*, 61–66. (In Chinese)

58. Cheng, G. *Research on the Mechanism of Rectangular Concrete-Filled Steel Tube Structure Stiffened with PBL*; Chang'an University: Xi'an, China, 2015. (In Chinese)

59. Tomii, M. Experimental studies on concrete filled steel tubular stub columns under concentric loading. In Proceedings of the International Colloquium on Stability of Structures under Static and Dynamic Loads, Washington, DC, USA, 17–19 May 1977; SSRC/ASCE: Washington, DC, USA, 1977.
60. *JTG/T D64-01-2015*; Specifications for Design and Construction of Highway Steel-Concrete Composite Bridge. China Communication Press: Beijing, China, 2015. (In Chinese)